Panoramic Holointerferometry

by D.R. Matthys, J.A. Gilbert and J. Puliparambil

ABSTRACT—This paper is the first to report on the quantitative evaluation of panoramic holointerferograms. In the experiment a collinear pair of panoramic annular lenses and an ion laser are used to illuminate and observe the inner walls of a circular pipe. A holographic image is obtained in the shape of an annulus showing the entire surround of the lenses. To produce the holointerferogram, a carrier is introduced by translating the pipe axially, and a line load is applied parallel to the system axis. The interference pattern of the carrier and deformation is then recorded with a CCD. This pattern is linearized by applying a two-dimensional mapping to correct the distortions introduced by the panoramic optical system and then the linearized pattern is analyzed in the usual way (phase mapping, carrier subtraction, phase unwrapping). The experimental results are excellent and demonstrate the unique value of panoramic annular lenses in making precision deformation mappings of the interior surface of pipes or cylinders.

Introduction

Several papers on the topic of radial metrology have been presented earlier on the use of a special panoramic annular lens (PAL) to make visual observations and/or precision measurements on the interior surfaces of rings or pipes.[1,12] Although a few of those earlier papers show the feasibility of making interferometric measurements with a PAL,[3,10,12] this paper is the first to report on the quantitative evaluation of panoramic holointerferograms.

Panoramic holointerferometry refers to the process of making a 360-deg double-exposure, real-time or time-averaged hologram of the inside of a cylindrical cavity wall using a panoramic annular lens. The PAL consists of a single piece of glass with spherical surfaces that produces a flat annular image of the entire surround of the optical axis of the lens with a field of view approximately 45-deg wide front to back. Since a virtual image is formed inside the PAL by a combination of reflection and refraction, a transfer lens must be employed to transfer the image to a sensor. A standard PAL imaging system is shown in Fig. 1. The PAL is almost afocal, and obtains an image from right up against the lens surface out to infinity. Objects to the front of the lens are imaged to the interior of the annulus and objects to the rear of the lens appear on the outer part of the annulus.

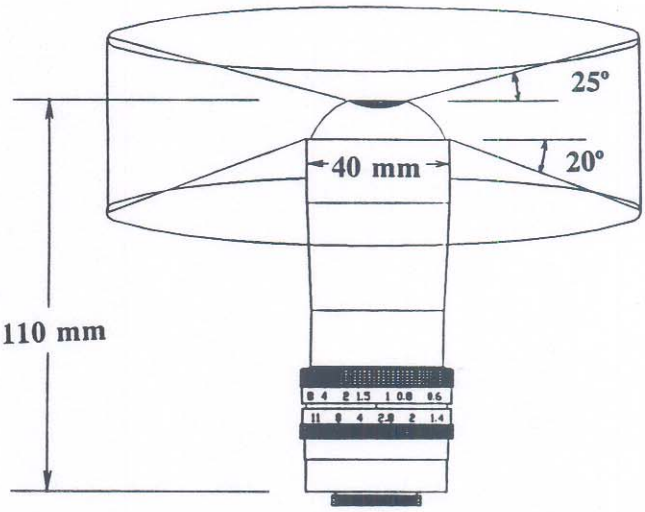

Fig. 1—A 38-mm diameter PAL imaging system. Figure provided courtesy of Optechnology, Inc., Gurley, AL

Direct visual interpretation of a PAL image is sometimes confusing for the unskilled observer and algorithms have been developed to allow the annular shaped images to be linearized for viewing and measuring purposes. The mapping used for this purpose maintains equal maximal dimensions by 'rolling' the annular image along its outer circumference and moving all the pixels between the contact point and the center of the image to a vertical line in the final rectangular image.[9] Next, because the annular image is not linear in the radial direction, a vertical stretching of the rectangular image is performed.[13]

This paper demonstrates that the PAL system and the linearization algorithms can be combined with the carrier-fringe method and phase unwrapping to perform quantitative analysis on panoramic holointerferograms. The experimental results are excellent and demonstrate the unique value of a PAL in making precision deformation mappings of the interior surface of pipes or cylinders.

Holographic Analysis

In Fig. 2, it is assumed that two opposing collinear PALs are aligned with their optical axes along the z direction; Cartesian (x, y, z) and cylindrical (r, θ, z) coordinate systems can be used to describe the object space. Coherent light is projected by one PAL from the source point S to a point P located on the inner wall of a cylindrical cavity. The image of P is observed by the second PAL at point O.

D.R. Matthys (SEM Member) is Professor, Physics Department, Marquette University, Milwaukee, WI 53233. J.S. Gilbert (SEM Member) is Professor, Department of Mechanical and Aerospace Engineering, University of Alabama, Huntsville, AL 35899. J. Puliparambil is Visiting Professor, Mathematics Department, Marquette University, Milwaukee, WI 53233.

Paper was presented at the 1993 SEM Spring Conference held in Dearborn, MI on June 7–9, 1993.

Original manuscript submitted: October 8, 1993. Final manuscript received: July 18, 1994.

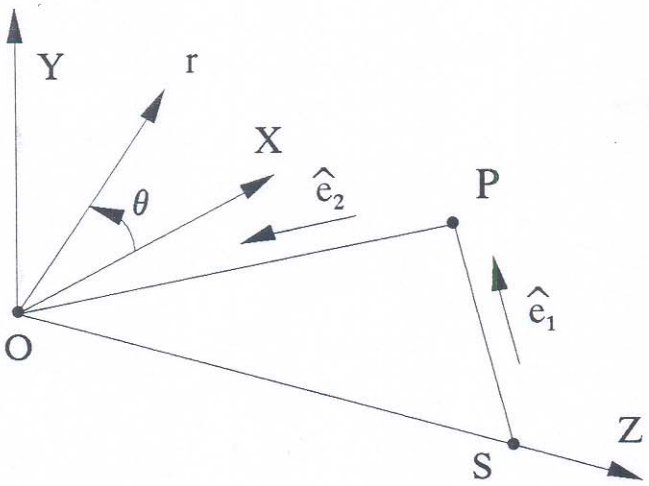

Fig. 2—Cartesian (x, y, z) and cylindrical (r, θ, z) systems used to describe object space

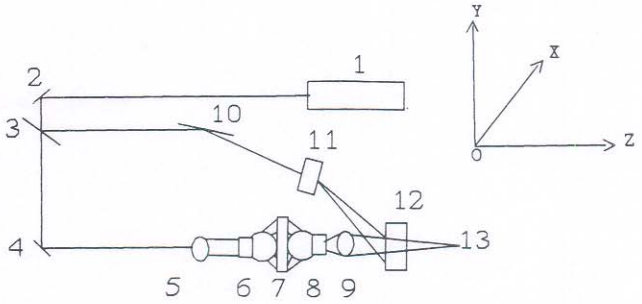

1. Laser
2. Mirror
3. Beam Splitter
4. Mirror
5. Collimating Lens
6. PAL
7. Pipe
8. PAL
9. Transfer Lens
10. Mirror
11. Spatial Filter
12. Thermoplastic Plate
13. Image Plane

Fig. 3—Experimental setup for recording real-time panoramic holointerferograms. A CCD camera is used to acquire images

To enable mathematical analysis, unit vectors $\hat{\mathbf{e}}_1$ and $\hat{\mathbf{e}}_2$ are shown in the direction of illumination and in the direction of observation, respectively. These vectors help in analyzing the holographic fringes produced when the reconstructed holographic image corresponding to an undeformed object and the same deformed surface are superposed. The change in path length between the two holographic recordings gives rise to a distribution of phase differences between the reconstructed wavefronts which results in areas of constructive or destructive interference and is seen as a set of light and dark fringes.

For the case shown in Fig. 2, the locations of fringes produced by this superposition are given by

$$n\lambda = (\hat{\mathbf{e}}_2 - \hat{\mathbf{e}}_1) \cdot \mathbf{d} = \mathbf{g} \cdot \mathbf{d} \qquad (1)$$

where n is the fringe order number and λ is the wavelength of the coherent light used to record and reconstruct the hologram. The component of displacement measured at each point depends upon the location of the source and on the point of observation; the displacement vector $\mathbf{d}$ is projected along the sensitivity vector $\mathbf{g}$ which lies along the angle bisector of $\hat{\mathbf{e}}_1$ and $\hat{\mathbf{e}}_2$. In general, the sensitivity vector lies along a different direction for each point in the field of view.

Although eq (1) yields the magnitude of the component of $\mathbf{d}$ along the direction of $\mathbf{g}$, its sign is uncertain. This sign ambiguity is troublesome and must be confronted in the data analysis. One approach is demonstrated in this paper; carrier fringes are introduced into a holointerferogram produced by deforming a circular pipe. The superposition produces a monotonically changing phase distribution along the interferogram. The sign of the displacement component is obtained when the carrier fringe pattern is subtracted from the holointerferogram in the spatial frequency domain.

Experimental

Experiments were performed on a vibration isolated table with the setup shown in Fig. 3. Two 38-mm (1.5-in.) diameter PALs were spaced at a distance of 3.175-mm (0.125-in.) apart and positioned with their optical axes aligned with the z axis of the coordinate system (see Fig. 2). A circular aluminum pipe with an inner radius R equal to 69.85 mm (2.75 in.) and a wall thickness of 3.0 mm (0.117 in.), was mounted on a kinematic stage and positioned around the PALs with its longitudinal axis also along z. The inner surface of the pipe was painted white. Then the pipe was placed in such a way that the two PALs could be centered inside it. Coherent light (λ = 514 nm) was projected onto the inner wall of a 50.8-mm (2.0-in.) long section of the pipe using a collimated beam passed through one of the PALs. An image of the pipe in its initial position was captured using a second PAL. A collector lens was used to convey the virtual image formed within the second PAL to a CCD camera and computer system. The reference beam reflected by the beam splitter was expanded through a spatial filter onto a thermoplastic holocamera positioned behind the collector lens.

Since the angle between the incident and the transmitted ray varies from +15 degrees to −15 degrees across the field of view, the direction of the sensitivity vector changes along the length of the pipe. This is illustrated in Fig. 4 which shows the sensitivity vectors for points located in the center and at the ends of the field of view. Figure 5 shows the fringe pattern recorded when the pipe was translated axially along the z axis, through a displacement w equal to 0.0038 mm (0.00015 in.). In this case, a zero-order fringe coincides with the path around the middle of the annular ring where the sensitivity vector is perpendicular to the displacement. The phase monotonically changes across the field of view.

Figure 6, on the other hand, shows an interferogram obtained when a vertical diametral load of 51 grams is applied to the pipe. The interpretation of this pattern requires the application of standard interferometric-analysis techniques such as phase-shifting and phase-stepping methods, hetrodyne holographic interferometry or carrier-fringe methods. Since the distortions inherent in the PAL image make this process difficult, they must be removed by the linearization

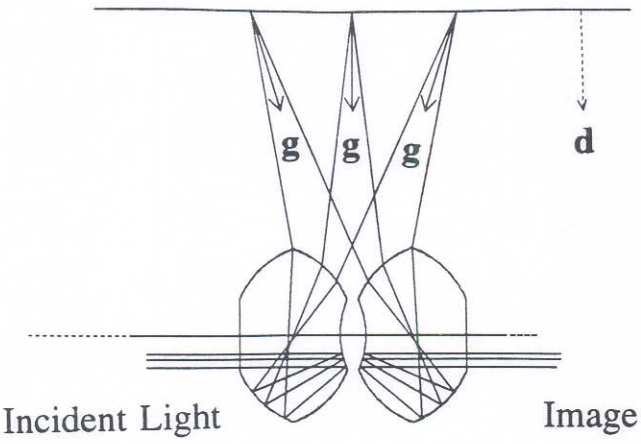

Fig. 4—Figure to show the direction of the sensitivity vector

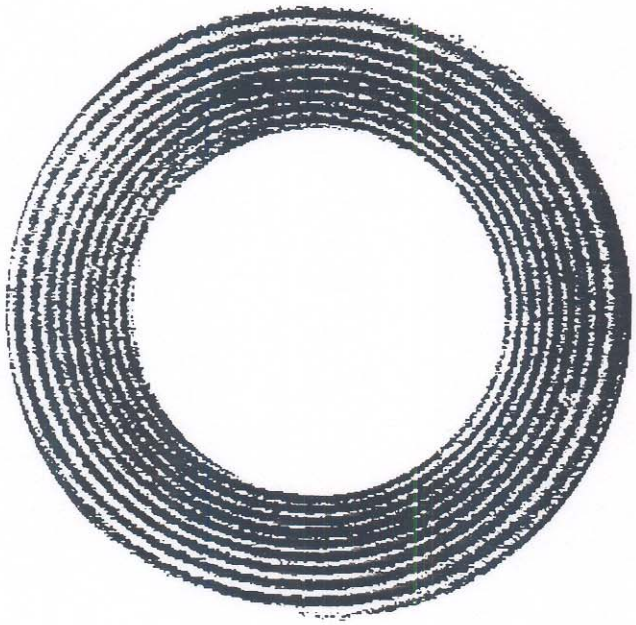

Fig. 5—Panoramic holointerferogram recorded when the pipe is translated in the axial *z* direction through 0.0038 mm

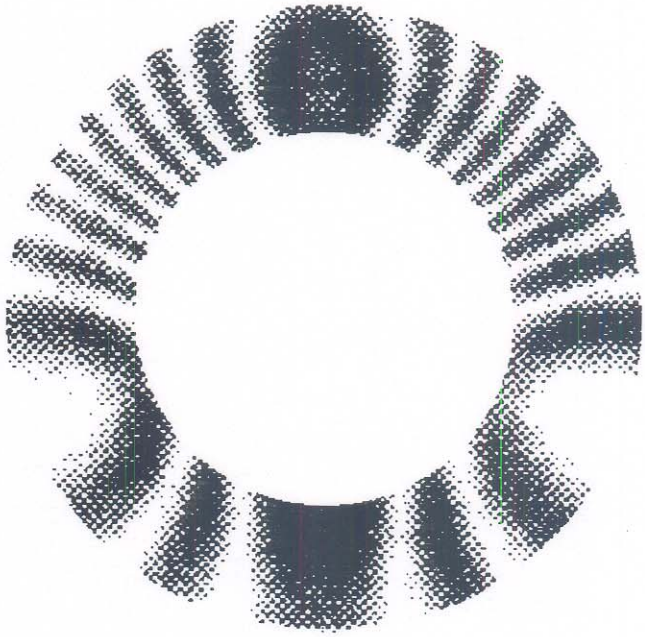

Fig. 6—Panoramic holointerferogram obtained by applying a vertical compression to the pipe by loading it with 51 grams

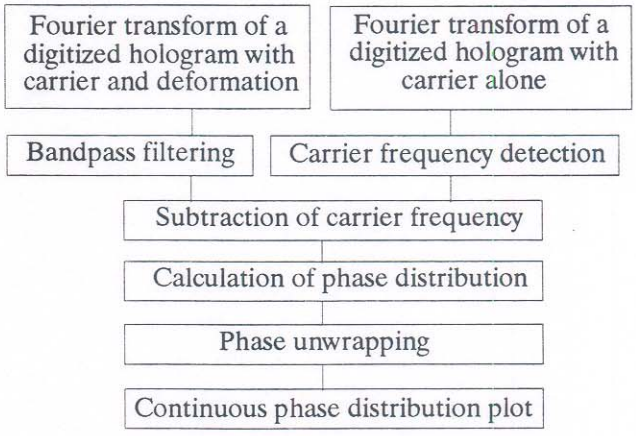

Fig. 7—Flow chart for phase unwrapping

procedure described earlier. Moreover, many of the standard fringe-analysis techniques will fail in those cases where the fringes form a closed loop because the same fringe will be encountered twice in going from one end of the interferogram to the other. This problem can be eliminated using the method of carrier fringes. The following section demonstrates how image linearization and the carrier-fringe method are used to obtain quantitative results for the deformation inherent in Fig. 6.

Data Analysis

A combination of image-digitization, image-processing, two-dimensional fast-Fourier transformation and subsequent computerized analysis is used in the data analysis. The procedure is given in the flow chart shown in Fig. 7.[14] The quantitative evaluation of the interference patterns mainly consists of the pointwise determination of the interference phase and of the sensitivity vectors. From the interference phase distribution and the sensitivity vectors, which are given by the geometrical arrangement of the optical components in the holographic setup, the displacement field is calculated. The method of carrier fringes makes use of the properties of Fourier transform to achieve this. The automated data analysis is performed with the help of a PL2500 Array Processor (by Eighteen and Eight Laboratory) and an Image-Pro Plus image processing system (by Media Cybernetics, Inc.).

The first step is to produce an interferogram having a monotonically changing phase distribution. This may be accomplished for the loaded pipe by superimposing the phase distributions corresponding to a carrier pattern, produced by translating the pipe along the z axis (see Fig. 5), with

the deformation produced by loading it (see Fig. 6). The resulting panoramic holointerferogram is shown in Fig. 8. The next step is to apply the linearization algorithms; the first quadrants of the images shown in Figs. 5 and 8 are shown in Figs. 9 and 10, respectively.

After linearizing the holointerferograms corresponding to the carrier and the carrier plus the deformation, the Fourier transform is applied to each of their quadrants. Each quadrant image is 295 pixels wide and 134 pixels high. The PL2500 array processor requires the signal to be a square array to apply the Fourier transform. So each quadrant is placed at the center of a square array of 512 × 512 video screen and saved into a file. This is accomplished using the ImagePro software program. All the pixels surrounding the quadrant are filled with zeros.

For direct FFTs, the input image file contains raw data in 8-bit unsigned integer format, while the PL2500 works on 32-bit floating point format. So the data format has to be converted after the data are transferred from the host PC to the PL2500 array processor. For a complex Fourier transform, the data should also be converted to complex values by inserting imaginary values of zero to form a complex data array for the FFT. For visual presentation, the data are shifted to move the origin of the spatial frequency domain to the center of the array.

Once the annular image has been linearized both tangentially and radially, standard[15–18] techniques of carrier introduction, phase unwrapping and noise reduction can be applied to obtain the phase distribution resulting from the surface displacements. The phase unwrapping algorithm is applied to the phase map obtained after the Fourier transform, bandpass filtering, and inverse Fourier transform of each of the quadrants is performed. Figure 11, for example, shows the phase map in the middle portion of the first quadrant after complete phase wrapping is done. Two-dimensional phase maps can also be plotted for the entire surface of each of the four quadrants and they show the displacement values on the inside surface of the pipe due to the applied load.

In order to show the displacement values inside the entire pipe the information from all four quadrants needs to be joined together. Figure 12 shows how the interferogram would look when the four quadrants are joined. This figure is made by changing the aspect ratio; the height of the picture is stretched so that it is possible to observe the overall shape of the linearized holointerferogram.

Actually, the phase unwrapping can be done manually since the fringe pattern is rather simple. The zero-order fringe is assigned to the point where the contact point between the surface and the pipe is located. At this point there is no displacement of the pipe. This occurs at the 270-deg point

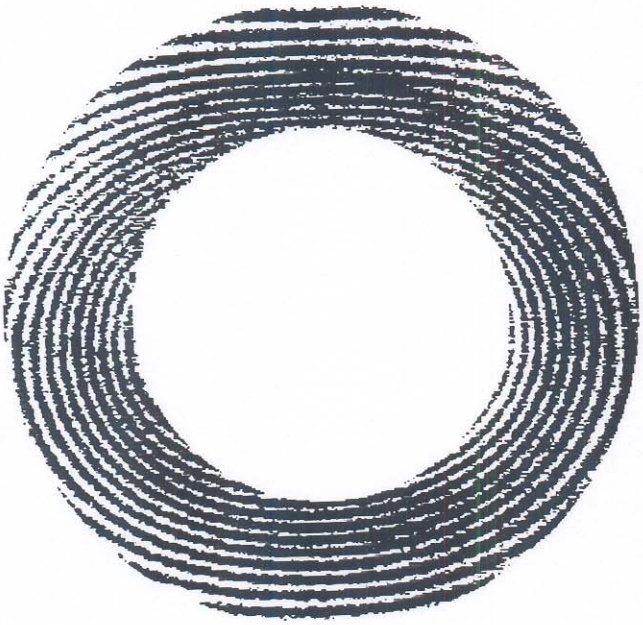

Fig. 8—Fringe pattern obtained when the pipe is subjected to diametral compression along with a translation in the axial *z* direction

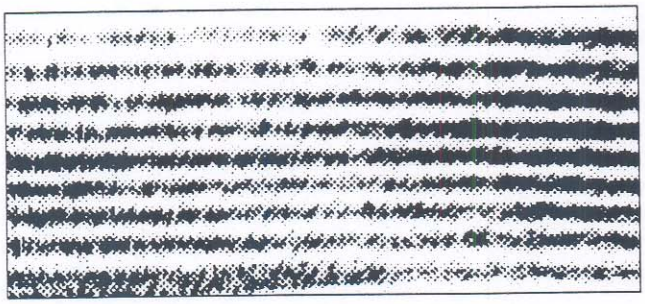

Fig. 9—Linearized version of the first quadrant of Fig. 5

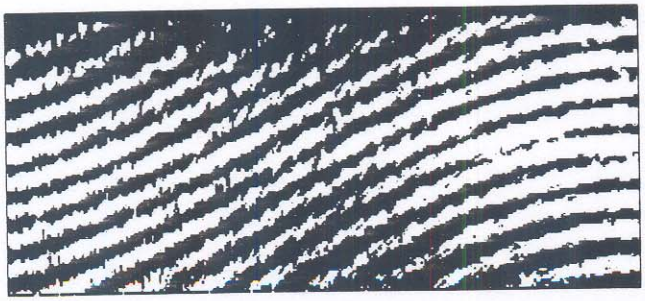

Fig. 10—Linearized version of the first quadrant of Fig. 8

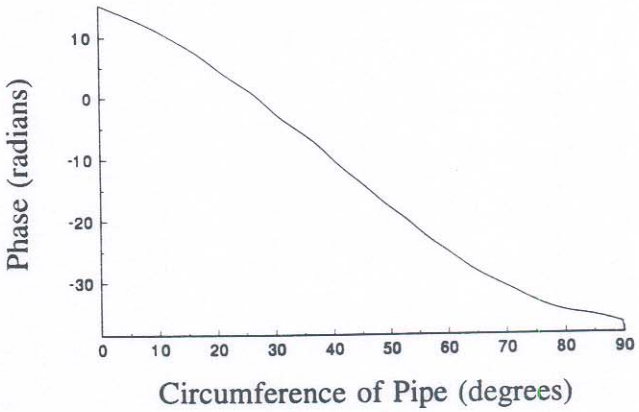

Fig. 11—The phase map of the middle portion of the first quadrant after complete phase unwrapping is done

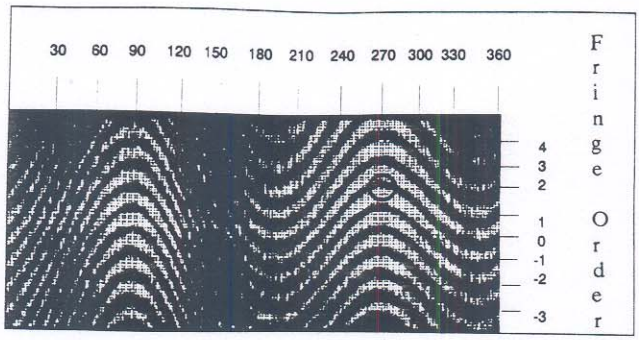

Fig. 12—An overall view of all the four quadrants joined together. Circle at 270 deg indicates fringe selected as zero order

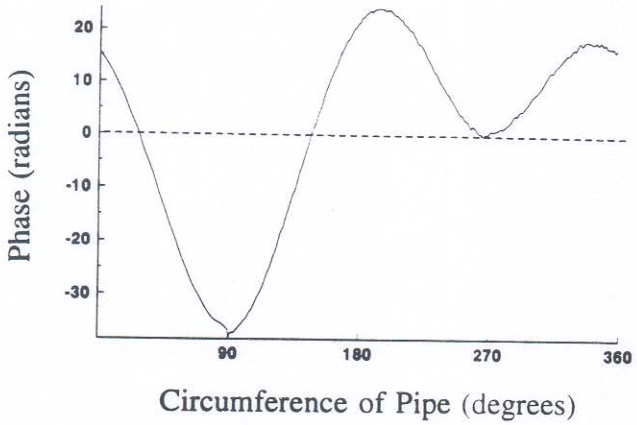

Fig. 13—Phase plot at the middle of the pipe around its circumference in degrees. Dotted line represents undeformed surface

on the circumference of the pipe. The third fringe from the top on this 270-deg point is selected for analysis and designated the zero order fringe. Its location is marked on Fig. 12 by a small circle. The fringes below it are numbered with increasing negative numbers and the fringes above it are numbered with increasing positive numbers. Now a horizontal line is drawn through the figure just touching the top of the chosen fringe at 270 deg. The total angle inside the cavity is 360 deg. At every 10 deg, the number of the fringe which crosses the horizontal line is recorded. A graph is drawn with the circumference of the pipe in degrees as abscissae and with fringe order numbers as ordinates. Figure 13 shows the phase map of the inside surface of the pipe around its circumference, the circumference of the pipe being in degrees. From this the nature of the displacement values around the circumference of the pipe is seen.

If the fringes were more complex in nature, it would have been very difficult to apply this method. So there is a need for automating this process. In order to do that, phase unwrapping is done and then the results for each of the four quadrants are joined together. However, a linearized image of the complete surface pipe is 1080 pixels and it is not feasible to display that big an image on most computer monitors as they do not have that much resolution. So the analysis is done a quadrant at a time and then the results are joined together after the phase unwrapping to view the 360-deg surround of the inner cavity surface.

The deformations caused by the diametral compression are of the order of a few wavelengths of light. So they cannot be plotted in their actual dimensions. They have to be multiplied by a scaling factor and then the shape of the deformation can be studied.

To demonstrate the shape of the pipe after deformation, it is assumed that the pipe is originally circular and can be represented by a circle of radius 5.08 cm (2 in.). If the deformation is magnified, then it can be superposed on this circle. It is seen in Fig. 13 that the maximum deformation produces a phase change of less than 50 radians. That value is taken as the maximum deformation. So to scale the maximum deformation to 6.35 mm (0.25 in.) a scale factor of 6.35 mm/50 radians (0.25 in./50 radians) is chosen. Now each phase change value on the circumference of the pipe as obtained from the phase unwrapping procedure is multiplied by this factor. Each of these values is either subtracted or added to the radius of the circle depending on the sign of the change. These values are plotted and the result is shown in Fig. 14. In Fig. 14, it is seen that the maximum vertical displacement occurs at the top and there is no displacement at the bottom where the pipe is in contact with the surface. On the other hand, the maximum horizontal displacement occurs at about 10 deg below the original center of the pipe.

Now from the phase unwrapping results it is found that the maximum phase change is 38.2 radians. For points in the image where the sensitivity vector is radial, the displacement u_r is

$$u_r = \frac{\Delta\phi\,\lambda}{4\pi\cos\theta} \tag{16}$$

where 2θ is the angle between the propagation vectors in the direction of illumination and observation.

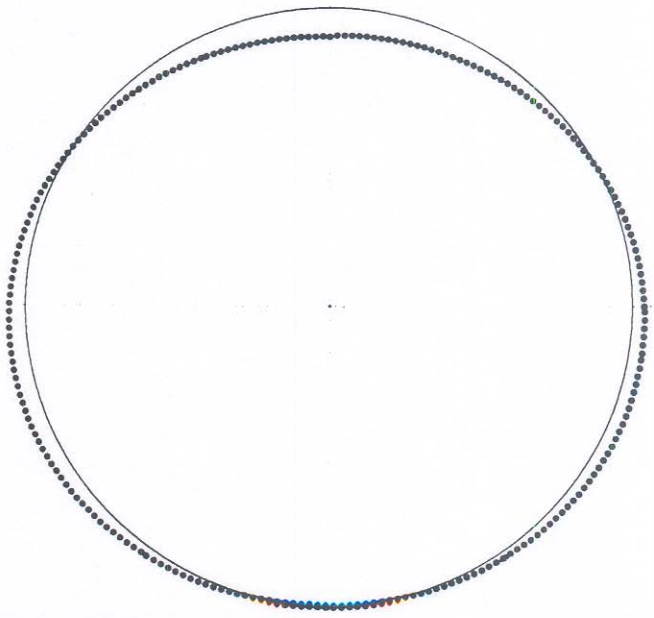

Fig. 14—Deformation of the pipe around its circumference. The deformation is exaggerated to make it visible

For the middle portion of the pipe the angle between these vectors is approximately 15 deg and the maximum deformation of the pipe is 1576.77 nanometers. Roark[19] discusses the deformation of a pipe that is subjected to diametral compression. The ratio of the change in the vertical to the change in the horizontal diameter is given as −1.0893. If the phase shifts shown in Fig. 14 are converted to displacements using eq (16), this ratio is −1.0852. The percentage of error from the theoretical value is less than 1 percent. The shape of the deformed section also agrees with that determined using artificial speckle and the method of digital correlation.[6]

In the section on holographic analysis, the effect of the sensitivity vector was discussed. Since the sensitivity vector changes across the field of view from +15 deg in the front to −15 deg at the back, an error factor (cos θ) is introduced into the radial displacement measurement. This error factor is maximum at the edges of the field of view where it is (1 − cos 15 deg), or 4 percent. At the center of the field of view where the sensitivity vector is vertical the error becomes zero. This error factor does not affect the way Roark's formulas are applied in this case, since Roark's result is a ratio which experiences the same change in both the denominator and numerator.

Conclusions

This paper has demonstrated that the method of phase unwrapping can be applied to obtain quantitative results from panoramic holointerferograms. The process uses an array processor along with a computer and is applied to linearized quadrants of panoramic images. These are later joined together to study the displacement field. The experimental results are consistent with theory and demonstrate the unique value of a PAL in making precision deformation mappings of the interior surface of pipes of cylinders.

References

1. Gilbert, J.A., Greguss, P., Lehner, D.L., Lindner, J.L., "Radial Profilometry," Proc. Joint BSSM/SEM Int. Conf. on Advanced Strain Measurement Tech. Whittles Publishing, 97–107 (Aug. 1987).

2. Greguss, P., Gilbert, J.A., Matthys, D.R., Lehner, D.L., "Developments in Radial Metrology," Proc. SPIE Int. Symp. on Opt. Eng. and Ind. Sensing for Advanced Manufacturing Tech. **954**, 392–398 (June 1988).

3. Gilbert, J.A., Greguss, P., Kransteuber, A.S., "Holo-interferometric patterns recorded through a panoramic annular lens," Proc. SPIE's Int. UNESCO Seminar on 3-D Holography, Vol. **1238**, entitled 3-D Holography '89, Kiev, USSR (Sept. 1989).

4. Matthys, D.R., Greguss, P., Gilbert, J.A., Lehner, D.L., Kransteuber, A.S., "Radial Metrology with a Panoramic Annular Lens," Proc. SPIE's 33rd. Annual Int. Symp. on Optical & Optoelectronic Appl. Sci. & Eng. (Aug. 1989).

5. Gilbert, J.A., Matthys, D.R., Greguss, P., "Optical Measurements Through Panoramic Imaging Systems," Proc. 1990 Int. Conf. on Hologram Interferometry & Speckle Metrology, 164–171 (Nov. 1990).

6. Matthys, D.R., Gilbert, J.A., Greguss, P., "Endoscopic Measurement Using Radial Metrology with Digital Correlation," Opt. Eng. **30**(10), 1455–1460 (1991).

7. Gilbert, J.A., Matthys, D.R., Lehner, D.L., Hendren, C.M., "Panoramic Imaging Systems for Nondestructive Evaluation," Proc. Third Conf. on Nondestructive Evaluation for Aerospace Requirements, (June 1991).

8. Gilbert, J.A., Matthys, D.R., Lehner, D.L., "Moire Measurements Using a Panoramic Annular Lens," Proc. SPIE's 1991 Int. Symp. on Optical & Optoelectronic Appl. Sci. & Eng. 202–209 (July 1991).

9. Matthys, D.R., Gilbert, J.A., Puliparambil, J., "Endoscopic Inspection Using a Panoramic Annular Lens," Proc. SPIE's 1991 Int. Symp. on Optical & Optoelectronic Appl. Sci. & Eng. 736–742 (July 1991).

10. Gilbert, J.A., Matthys, D.R., Hendren, C.M., "Displacement Analysis of the Interior Walls of a Pipe Using Panoramic Holo-interferometry," Proc. SPIE's 1991 Int. Symp. on Optical & Optoelectronic Appl. Sci. & Eng. 128–134 (July 1991).

11. Beshears, R.D., Gilbert, J.A., Matthys, D.R., "Non-destructive Examination of Rocket Motor Components," Proc. 1992 Conf. on Advanced Earth-To-Orbit Propulsion Technology (May 1992).

12. Lindner, J.L., Gilbert, J.A., "Modal Holographic Interferometry Utilizing the Panoramic Annular Lens," Proc. 11th Int. Modal Analysis Conf. (IMAC), (Feb. 1993).

13. Puliparambil, J., "Panoramic Imaging and Holographic Interferometry Using a Panoramic Annular Lens," PhD Doctoral Diss., Marquette Univ., Physics Dept. 24–36 (1982).

14. Guo, D., "Automated Evaluation of Holographic Interferograms by Combining Fourier Transform and Phase Shift Techniques," Master's Thesis, Marquette Univ., Physics Dept., 34–37 (1989).

15. Sciammarella, C.A., "A Numerical Technique of Data Retrieval from Moire or Photoelastic Patterns," Proc. Pattern Recognition Studies, 92–101 (1967).

16. Takeda, M., Ina, H., Kobayashi, S., "Fourier Transform Method of Fringe-pattern Analysis for Computer-based Topography and Interferometry," J. Opt. Soc. of Amer., **72** 156–160 (1982).

17. Matthys, D.R., Dudderar, T.D., Gilbert, J.A., "Automated Analysis of Holointerferograms for the Determination of Surface Displacement," EXPERIMENTAL MECHANICS, **28**(1), 86–91 (1988).

18. Sciammarella, C.A., Bhat, G., "Two Dimensional Fourier Transform Methods from Fringe Pattern Analysis," Proc. VII Int. Cong. on Exp. Mech., 1530–1538 (June 1992).

19. Young, W., Roark's Formulas for Stress and Strain, McGraw-Hill, New York, 262–263 (1989).